geosciences

MDPI

Article

Assessing the Use of Electrical Resistivity for Monitoring Crude Oil Contaminant Distribution in Unsaturated Coastal Sands Under Varying Salinity

Margaret A. Adeniran [1,2,*], Michael A. Oladunjoye [1,2] and Kennedy O. Doro [3,4,*]

[1] Pan African University, Life and Earth Sciences Institute (Including Health and Agriculture), Ibadan 200005, Nigeria; ma.oladunjoye@yahoo.com
[2] Department of Geology, University of Ibadan, Ibadan 200005, Nigeria
[3] Department of Environmental Sciences, University of Toledo, 2801 W Bancroft Street, Toledo, OH 43606, USA
[4] Science for Development Research and Teaching Initiative, Lagos 100213, Nigeria
* Correspondence: adeniranmargaret93@gmail.com (M.A.A.); kennedy.doro@utoledo.edu (K.O.D.)

Abstract: Monitoring crude oil spills in coastal areas is challenging due to limitations in traditional in situ methods. Electrical resistivity imaging (ERI) offers a high-resolution approach to monitoring the subsurface spatial distribution of crude oil, but its effectiveness in highly-resistive, unsaturated coastal sands with varying salinity remains unexplored. This study assessed the effectiveness of ERI for monitoring crude oil spills in sandy soil using a 200 × 60 × 60 cm 3D sandbox filled with medium-fine-grained sand under unsaturated conditions. Two liters of crude oil were spilled under controlled conditions and monitored for 48 h using two surface ERI transects with 98 electrodes spaced every 2 cm and a dipole–dipole electrode array. The influence of varying salinity was simulated by varying the pore-fluid conductivities at four levels (0.6, 20, 50, and 85 mS/cm). After 48 h, the results show a percentage resistivity increase of 980%, 280%, 142%, and 70% for 0.6, 20, 50, and 85 mS/cm, respectively. The crude oil migration patterns varied with porewater salinity as higher salinity enhanced the crude oil retention at shallow depth. High salinity produces a smaller resistivity contrast, thus limiting the sensitivity of ERI in detecting the crude oil contaminant. These findings underscore the need to account for salinity variations when designing remediation strategies, as elevated salinity may restrict crude oil migration, resulting in localized contaminations.

Keywords: crude oil contaminant; coastal sands; subsurface monitoring; electrical resistivity imaging

Citation: Adeniran, M.A.; Oladunjoye, M.A.; Doro, K.O. Assessing the Use of Electrical Resistivity for Monitoring Crude Oil Contaminant Distribution in Unsaturated Coastal Sands Under Varying Salinity. *Geosciences* **2024**, *14*, 308. https://doi.org/10.3390/geosciences14110308

Academic Editor: Umberta Tinivella

Received: 14 September 2024
Revised: 9 November 2024
Accepted: 12 November 2024
Published: 14 November 2024

1. Introduction

Crude oil contamination in coastal areas such as the Niger Delta region of Nigeria has received increased attention in recent decades due to its significant impact on the environment and public health. This concern is primarily driven by extensive hydrocarbon exploration and production activities in these regions [1]. Continuous crude oil spillage in coastal areas presents a severe risk to the local ecosystem, groundwater resources, soil quality, and biodiversity [2,3]. Coastal environments, in contrast to terrestrial areas, present unique challenges, such as their complex characteristics [4], which include their dynamic depositional processes, saltwater intrusion and overwash, and complex groundwater flow systems. These characteristics are mainly influenced by tidal action, flooding, and sea level rise [5,6].

Crude oil is an organic material that does not dissolve in water, and its migration into the subsurface depends on the physical and biochemical properties of the host material [7,8]. The behavior of crude oil in coastal sands under unsaturated conditions is complex and influenced by the hydrophobic nature of crude oil, its interaction with saline porewater in the sediment, and tidal action along the coast [9]. When released into the subsurface, crude oil displaces conductive porewater with non-conductive crude oil, altering the bulk

subsurface physical properties [10]. Saltwater also alters the physiochemical properties of the sand [11]. For example, high salinity can affect soil wettability and permeability, thus influencing the migration and dispersion of crude oil contaminants [12,13]. Salinity variation in porous media in coastal regions may result from tidal action or sea-level rises, which can cause saltwater overwash on land [14,15]. In many natural and engineered crude-oil-contaminated systems, understanding the subsurface physical properties such as soil texture, degree of water saturation, and salinity is significant in characterizing the distribution of the contaminant plume and monitoring its remediation [16].

The effective remediation of coastal areas contaminated by crude oil spills requires obtaining information about the soil properties and the spatial and temporal distribution and concentration of the crude oil contaminant within the subsurface [17]. This is usually achieved by carrying out a detailed subsurface site characterization, which involves collecting soil samples from soil cores and analyzing them in the laboratory for the soil's physical, chemical, and biological properties, including soil texture, moisture content, organic matter content, redox potential, microbial population, flow properties, and the concentration of the crude oil [18,19]. Recent technological advances have also led to an increase in the use of in situ sensors and testing approaches for monitoring the aforementioned state changes [20]. However, both soil sampling and in situ monitoring, as in most soil characterization problems, provide discrete data that are limited to characterizing the spatial and temporal distribution of the subsurface properties and the crude oil [21]. Additionally, these methods are invasive and could easily lead to cross-contamination [22]. Geophysical methods, including electrical resistivity or conductivity imaging, provide a fast, non-destructive approach for obtaining soil physical property (e.g., resistivity or its inverse, conductivity) distribution, which can be related to the soil hydraulic or biogeochemical properties of interest [23–25]. Also, when released into the subsurface, crude oil increases the bulk electrical resistivity of the porous media by directly displacing conductive porewater and replacing it with non-conductive crude oil [10]. Hence, geophysical methods, including electrical resistivity imaging (ERI), are sensitive to the presence of crude oil and can be used to characterize their spatial distribution within the subsurface [26,27]. Hence, when combined with soil sampling, laboratory analysis and in situ monitoring, geophysical methods can be used to image the subsurface to provide information on the soil properties and contaminant distribution [28,29]. However, there are limited studies assessing the sensitivity and limitation of electrical resistivity for imaging the presence and distribution of crude oil contaminants in coastal sands.

In a previous study, Adeniran et al. [30] showed that ERI is sensitive to the presence of crude oil contaminants in salt-impacted coastal sand. This study was, however, limited to saturated conditions and did not consider variation in the soil salinity. Naturally, the coastal sand in the Niger Delta region of Nigeria is characterized by high spatial and temporal variation in the degree of their water saturation depending on their location along the coast, groundwater levels, precipitation, and tidal fluctuation [31]. Also, significant variation in salinity has been reported [32,33], even under site-specific conditions [34–36]. Given this context, it is important to assess the sensitivity and limitation of ERI for characterizing and monitoring the distribution of crude oil within coastal sands under unsaturated conditions and varying salinity.

In this study, we present the results of a controlled laboratory sandbox experiment for assessing the effects of varying salinity on the use of ERI for monitoring the distribution of crude oil contaminants in coastal sandy soil. We simulated variation in soil salinity by changing the pore fluid conductivity and repeated the resistivity measurements. The results of this study will provide critical insights into the effectiveness and limitations of using ERI as a non-invasive geophysical method for detecting and monitoring the distribution of crude oil contaminants within coastal areas. An improved understanding of the strength and limitation of ERI will contribute to a more accurate and effective characterization and monitoring of contamination in coastal settings, ultimately contributing to an efficient remediation strategy.

2. Materials and Methods

This study involves a laboratory setup for a controlled release of crude oil, simulating a spill at the surface, and assessing the efficacy of electrical resistivity to image the distribution of the crude oil within an unsaturated coastal sand. The experimental setup includes a controlled sandbox with unsaturated soil with varying salinity and an electrical resistivity system and electrode setup for monitoring the distribution of the crude oil over time.

2.1. Sandbox Experimental Setup and Simulated Crude Oil Spill

We used a 200 cm × 60 cm × 60 cm sandbox made of 10 mm plexiglass (Figure 1a) for the experiment. For this study, we filled the sandbox with medium-fine-grained sand, which is the typical grain size distribution of sand found in the coastal areas of Nigeria. The experiments simulated an unsaturated coastal sandy soil condition with variable salinity typical of conditions along the coastal regions of Nigeria. For each experiment, the main chamber of the sandbox (Figure 1b) was filled with medium-to-fine-grained sand up to a height of 40 cm. The upper 20 cm were preserved as headspace to maintain aerobic conditions. A detailed description of the construction of the plexiglass sandbox and the experimental setup was presented by Adeniran et al. [30]. To initiate each experiment, 20 kg of sand was manually oversaturated with the saturating fluid (NaCl solution with a constant salinity) to allow an even fluid distribution and avoid unintended stratification across the system. The salt solution was achieved by increasing the amount of salt diluted in water until the desired fluid electrical conductivity value was achieved. The measurement of fluid electrical conductivity was used as a proxy for salinity concentration. The sandbox was then filled with moist sand up to a 40 cm mark in a 5 cm stepwise fashion to minimize the effect of differential soil compaction. After filling the sandbox with sand, we flushed the system with a saltwater solution of known salinity. After flushing, the setup was allowed to drain overnight for about 12 h and thereafter left to settle for another 24 h. This sought to ensure that the pore spaces were only partially filled with water to differentiate the soil condition from a saturation soil condition where the pore spaces are completely filled with water. Four different fluid electrical conductivities were used for each of the four experimental steps, i.e., 0.6 mS/cm, 20 mS/cm, 50 mS/cm, and 85 mS/cm. The choice of the fluid electrical conductivities used represents a range of values reported in the literature for different coastal areas in Nigeria [32–36].

The crude oil spillage was simulated by creating a gradual seepage of crude using a perforated bowl (15 cm by 10 cm) positioned at the top approximately 60 cm from the left border of the sandbox's inner chamber. The crude oil used is an Escravos crude oil from Warri Delta State, in the Niger Delta region of Nigeria, with an API ranging from 33 to 33.5 degrees and a sulfur concentration between 0.15 and 0.18%. Two liters of crude oil was poured into the perforated bowl located at the top of the sandbox and allowed to gradually seep into the sand unit (Figure 1b). Before the spillage, background electrical resistivity measurements (described below) were taken, while six cycles of measurements were conducted after the simulated spill over a 48 h duration.

2.2. Electrical Resistivity Measurement

Four laboratory experiments with varying salinity were conducted to assess the effect of varying salinity on using non-invasive ERI to monitor the crude oil spillage within the sandbox. The electrical resistivity method involves injecting a direct current or low frequency alternating current (I) into a medium using a pair of current electrodes and measuring the corresponding potential difference (V) using a second pair of potential electrodes [37]. The relationship between the potential difference and the injected current is described by Ohm's law (Equation (1)):

$$I = \frac{\Delta V}{R} \quad (1)$$

where R is a constant of proportionality known as the electrical resistance (Ohms). The resulting electrical resistance is converted into apparent resistivity using the following relationship:

$$\rho = R * k \quad (2)$$

where ρ = resistivity of the subsurface (Ω-m) and k = Geometric factor or electrode configuration constant, which depends on the spacing and geometry of the electrodes. The concept of electrical resistivity imaging involves the use of four electrodes to measure the electrical resistivity distribution along a transect.

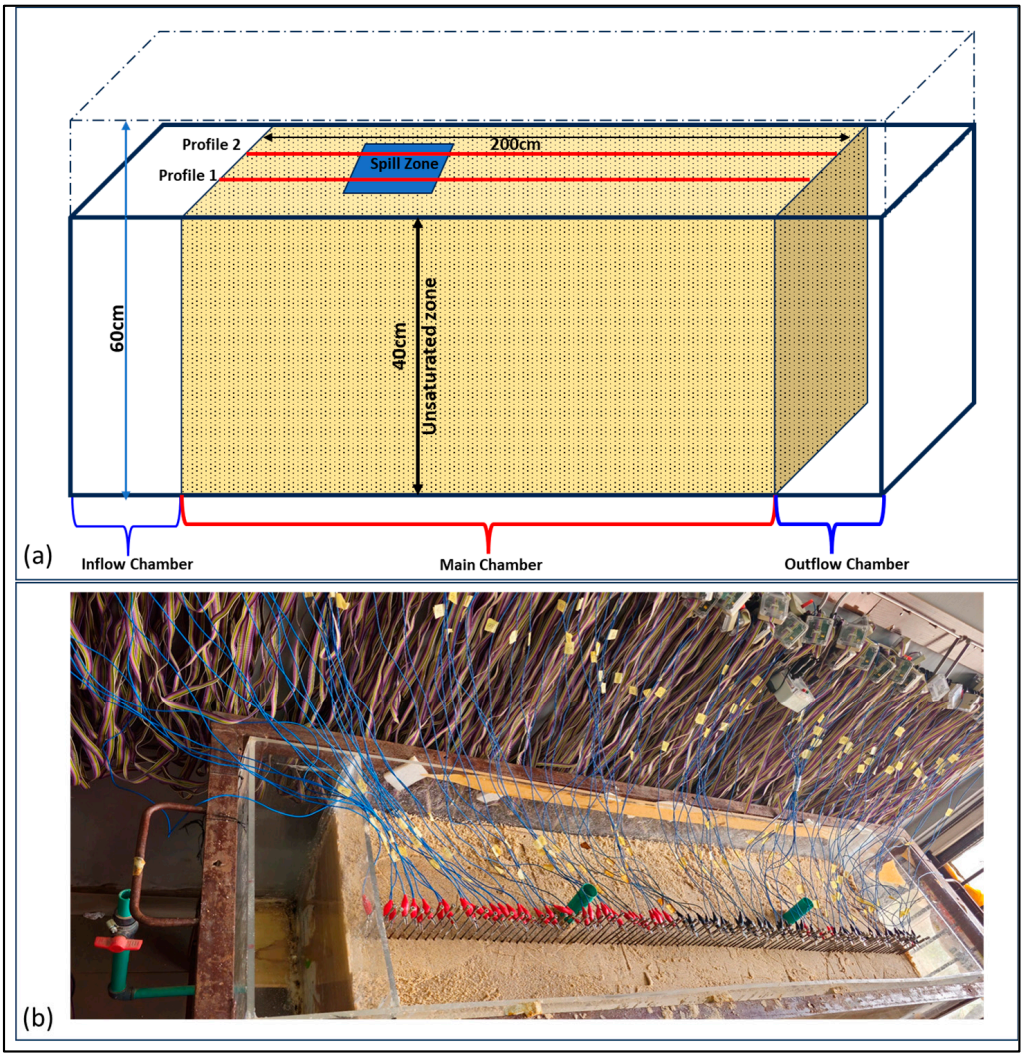

Figure 1. (**a**) Experimental design of the sandbox showing an inflow and outflow chamber on the left and right sides; (**b**) Laboratory setup of the sandbox and the geophysical measurements with the cables connected to 98 electrodes. The electrodes are spaced 2 cm apart along a 198 cm profile length.

The electrical resistivity measurements were conducted using an automated 4-point 10 W earth resistivity meter (Schwab Research Technology, Achim, Germany) with 98 electrodes with a unit electrode spacing of 2 cm. Before commencing the simulated crude oil spill experiment, two profiles (Profiles 1 and 2), with a profile length of 198 cm and inter-profile spacing of 12 cm, were first established. Electrical resistivity measurements were performed using a fabricated stainless-steel electrode, measuring 10 cm long. A series of electrical resistivity data were collected before, during, and after the crude oil spillage. The experimental setup took approximately fifteen minutes for each profile. For each measurement, we used a current injection of 0.1 mA and three measurement cycles with a

2% measurement error. A total of 1929 apparent resistivity data points were collected along each profile, which took about 30 min and averaged 0.9 s per data point. For the crude oil simulation, Profile 1 was acquired immediately after the crude oil spill, while Profile 2 was acquired 45 min post-spill. The resistivity measurement along the two profiles were alternated using the same system, resulting in a total measurement timeline of 75 min for each measurement cycle. Reciprocal measurements were conducted during data acquisition prior to and after the crude oil spill to assess the accuracy of the resistivity measurements. This involved reversing the current and potential electrode quadrupoles to verify the consistency and reliability of the resistivity data.

A total of 28 electrical resistivity measurements were taken, seven per profile for each salt concentration over 48 h for each experimental cycle. However, only measurements taken at the time (0, 1, 8.5, 24, and 48 h) for profile 1 and (0, 2.15, 9.45, 24.15, 25.15, and 49.15 h) for profile 2 were presented in the Section 3. The quality of the data obtained was accessed by estimating the reciprocal errors (i.e., the difference between the forward and reversed quadrupole measurements using the same electrode pair). Electrode pairs with a reciprocal error > 10% were rejected, resulting in less than 5% of the data rejected for failing to meet the reciprocal error criteria. The resistivity data were inverted using the ResIpy inversion framework, which provides a graphical user interface (GUI) for implementing an R2 inversion code based on a Gauss–Newton numerical scheme. The individual 2D resistivity transect data were first inverted using the standard inversion routine [38] following an approach described by Doro et al. [39]. Subsequently, we employed a difference inversion approach [40] to conduct a time-lapse resistivity inversion of the repeated resistivity data along the same transect. The R2t code, which is also integrated into the ResIpy inversion framework, was employed to emphasize the resistivity differences between each subsequent measurement timestep. In all inversions, the resistivity model converged after two to three iterations with a root mean square (RMS) error value ranging from 0.9 to 1.3 and the normalized error model ranging from −3 to 3.

3. Results

3.1. Electrical Resistivity Imaging of the Simulated Spill

The background resistivity inversion results for the unsaturated sands without any crude oil spill, measured across four different pore fluid salinity levels, consistently show a two-layer resistivity distribution across the two profiles (Figure 2). This two-layer resistivity distribution is puzzling as we expected the moist and relatively homogeneous sand to give a single resistivity layer. We, however, attribute this to a gravity-induced moisture content stratification within the homogeneous sand when left to settle, with the moisture content higher at the lower section of the sandbox than the upper section and the sand at the upper section being relatively dryer. The upper layer (top 0.2 m) has resistivity values ranging from 600 to 9000 Ωm, 39–225 Ωm, 8–91 Ωm, and 2–28 Ωm for salinity levels of 0.6, 20, 50, and 85 mS/cm, respectively. Beneath this layer is a low-resistivity layer that extends from 0.2 to 0.4 m. The resistivity values range from 100 to 1000 Ωm, 11–19 Ωm, 2–5 Ωm, and 2–5 Ωm for 0.6, 20, 50, and 85 mS/cm, respectively. The contrast between the upper highly resistive layer and deeper low resistivity layer yields an approximate ratio of 90%, 91%, 91%, and 77% for 0.6, 20, 50, and 85 mS/cm, respectively.

For the 0.6 mS/cm porewater salinity, the 2D ERI sections exhibit temporal variation in resistivity over 48 h (Figure 3). Initially, within one-hour post-spillage, the resistivity increased within the spill zone down to a depth of 0.4 m, with an average value of 6000 Ωm across the two profiles. This increase in resistivity continues over the next 8 h, reaching an average of 7500 Ωm. The 24 h post-spillage resistivity continues to increase, reaching a maximum of 8000 Ωm after 48 h.

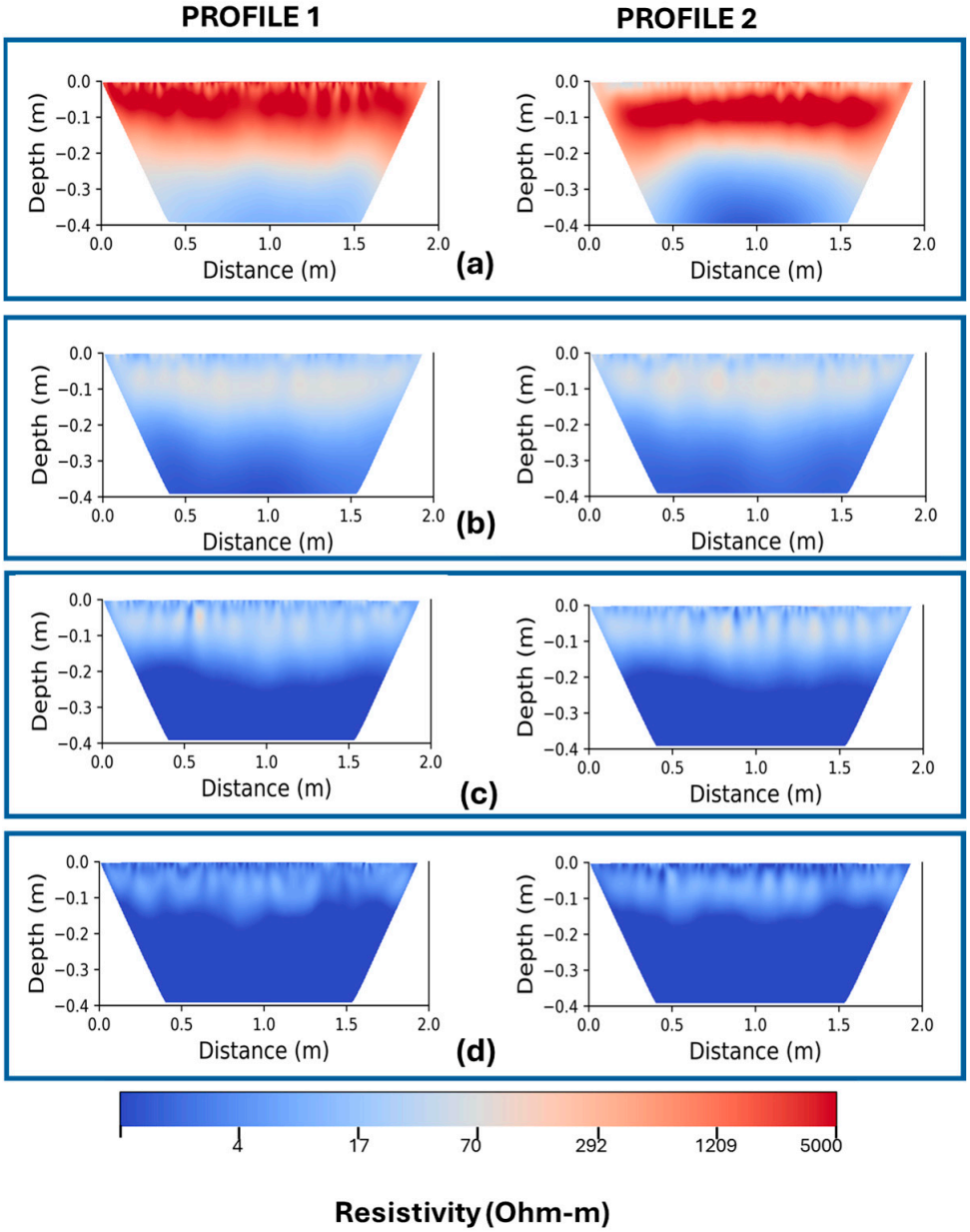

Figure 2. Two-dimensional resistivity inversion results for (**a**) unsaturated sand with a concentration of (0.6 mS/cm), iteration no. = 3, RMS = 1.12; (**b**) unsaturated salt-impacted sand with a concentration of (20 mS/cm), iteration no. = 3, RMS = 1; and (**c**) unsaturated salt-impacted sand with a concentration of (50 mS/cm), iteration no. = 3, RMS = 1.2; (**d**) unsaturated salt-impacted sand with concentration of (85 mS/cm), iteration no = 3, RMS = 1.5.

Figure 4 shows the 2D resistivity profile for a 20 mS/cm concentration. One hour after the spill, the resistivity within the spill zone increased to an average of 261 Ωm at a depth of 0.2 m, an average reduction of 2000% in resistivity compared to 0.6 mS/cm concentration. Unlike the 0.6 mS/cm concentration, where resistivity continues to increase after 8 h, for 20 mS/cm concentration, the resistivity value reduced up to an average of 192 Ωm. After this initial drop, resistivity values rose again after 24 h, reaching 249 Ωm, and increasing to a maximum of 315 Ωm after 48 h. At a distance of 1.5 m at a depth of 0.2 m, a reduction in resistivity from 61 Ωm to 30 Ωm was observed. In contrast, resistivity remains relatively constant at a depth of 0.35 m for the first 8 h before gradually increasing from 12 Ωm to 45 Ωm after 48 h.

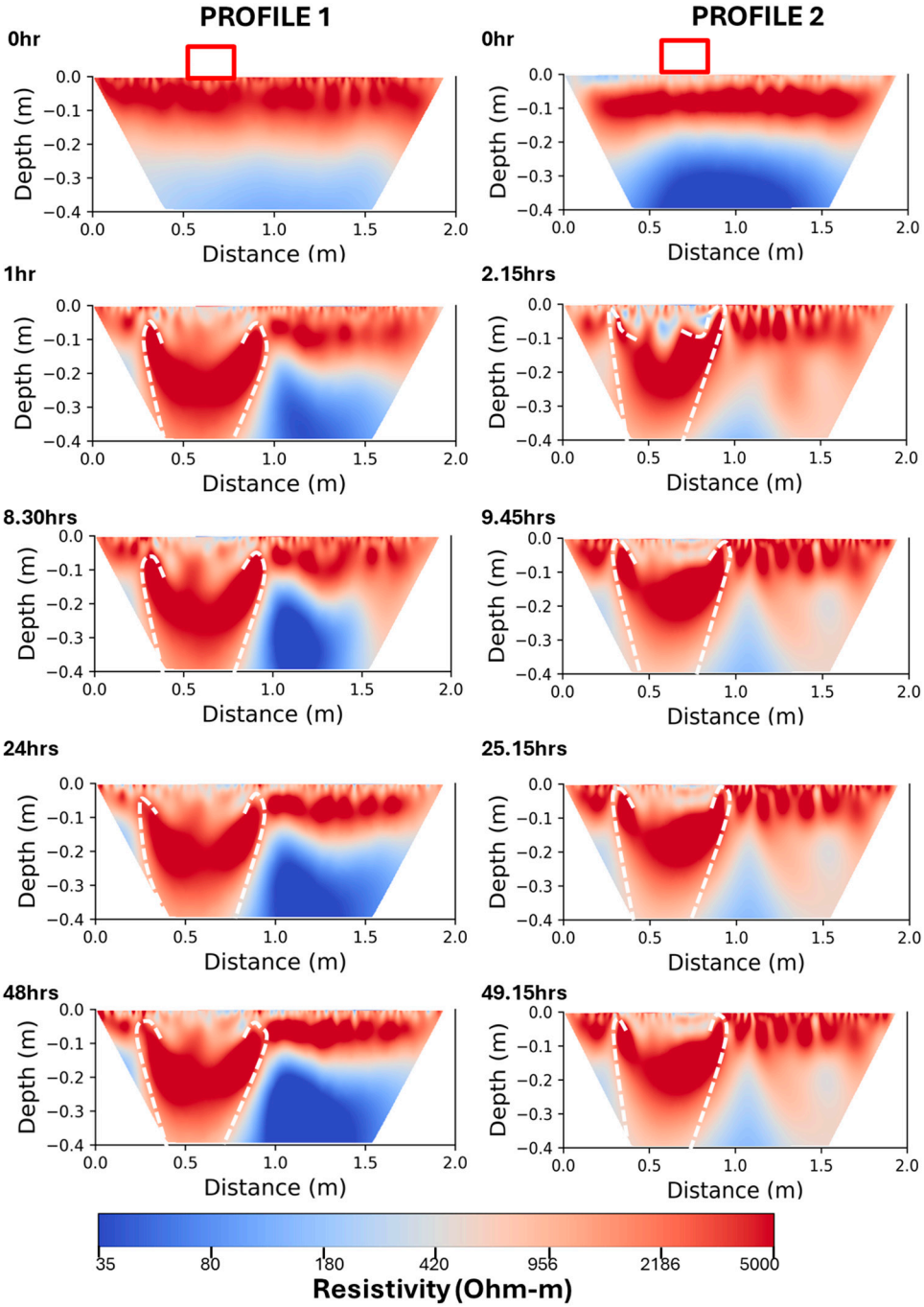

Figure 3. Two-dimensional resistivity inversion result taken across Profile 1 and Profile 2 for unsaturated sand during the crude oil spillage experiment. Five separate measurements were taken at different times for over 49.15 h using the dipole–dipole array. The red box at the top of the profile shows the crude oil spill surface location between x = 60 cm and x = 75 cm. The white-dashed lines show the left and right boundaries of the crude oil contaminant front.

Figure 5 shows the resistivity profile for the 50 mS/cm porewater salinity. One-hour post-spill, the resistivity values at 0.2 m depth increased from 15 Ωm to 34 Ωm under the spill zone. After eight hours, the resistivity falls to 26 Ωm, reflecting the trend in the 20 mS/cm concentration, where a decline was also noted following the first spike. After 24 h, the resistivity remains stable for the rest of the experiment. A notable increase in resistivity was observed at 0.1 m depth with a resistivity increase from 85 Ωm to 102 Ωm about 1 h after the spill, and reaching a maximum of 206 Ωm after 48 h. At a depth of

0.1 m, the resistivity was relatively constant at distances between 1.0 and 1.5 m, with values averaging 80 Ωm throughout the experiment. This stability contrasts the more dynamic resistivity variations observed in the 0.6 mS/cm and 20 mS/cm profiles at similar distances. Though the latter two showed more variability, the 50 mS/cm concentration resistivity maintains a low average value of 4.5 Ωm at depths between 0.2 and 0.35 m.

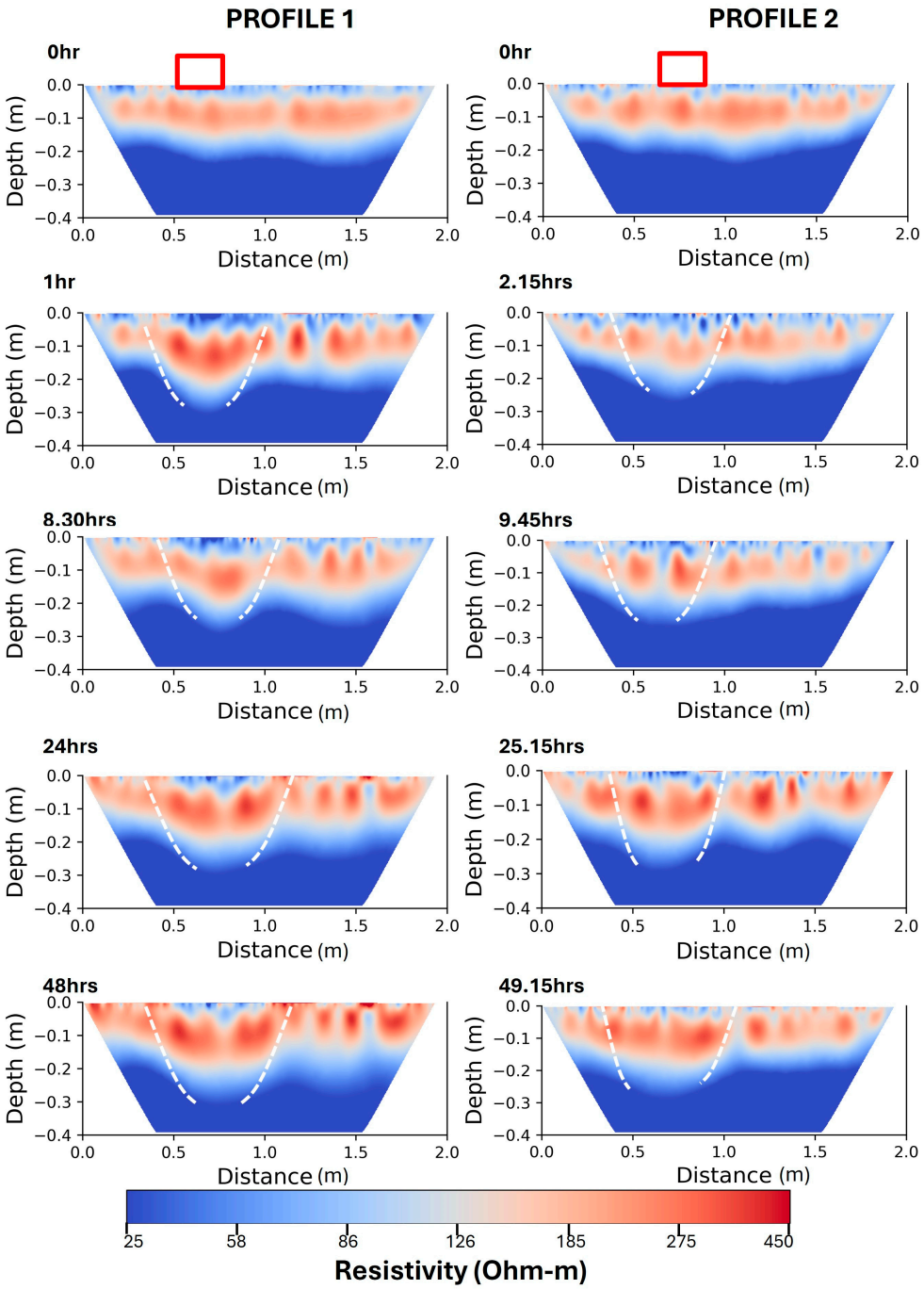

Figure 4. Two-dimensional resistivity inversion results across Profiles 1 and 2 for unsaturated salt-impacted sand with a salinity of 20 mS/cm during the crude oil spill experiment. Five separate measurements were taken at different times for over 49.15 h using the dipole–dipole array. The red box at the top of the profiles show the crude oil spill surface location between x = 60 cm and x = 75 cm. The white-dashed lines show the left and right boundaries of the crude oil contaminant front.

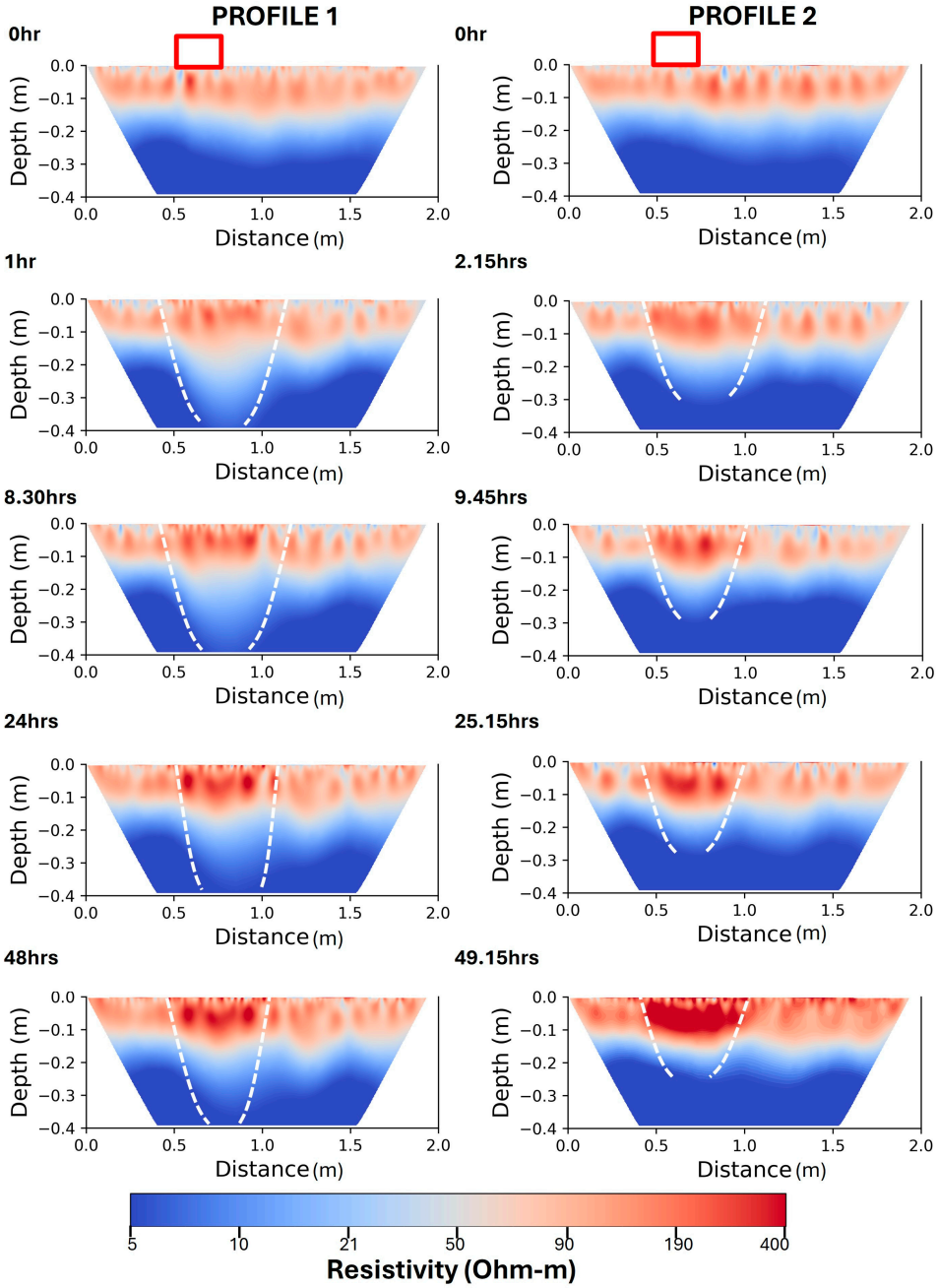

Figure 5. Two-dimensional resistivity inversion results taken across Profiles 1 and 2 for unsaturated salt-impacted sand with a salt concentration of 50 mS/cm during the crude oil spill experiment. Five separate measurements were taken at different times for over 49.15 h using a dipole–dipole array. The red box at the top of the profile shows the crude oil spill surface location between x = 60 cm and x = 75 cm. The white-dashed lines show the left and right boundaries of the crude oil contaminant front.

Similarly to the 50 mS/cm concentration, the notable increase in resistivity was restricted to 0.1 m depth. One hour after the spill, the resistivity directly under the spill zone increased to an average of 26 Ωm at a depth of 0.1 m (Figure 6). The resistivity remained relatively stable after the initial increase, reaching a maximum value of 39 Ωm after 24 h, and remained at this level for the next 48 h. At 1.0 to 1.5 m, the resistivity initially decreased from 34 Ωm to 20 Ωm within the first hour. Subsequently, over 48 h at a depth of 0.1 m, it consistently increased to 39 Ωm. Although the magnitudes of the values are somewhat smaller, the concentration of 50 mS/cm indicates a gradual increase to some extent.

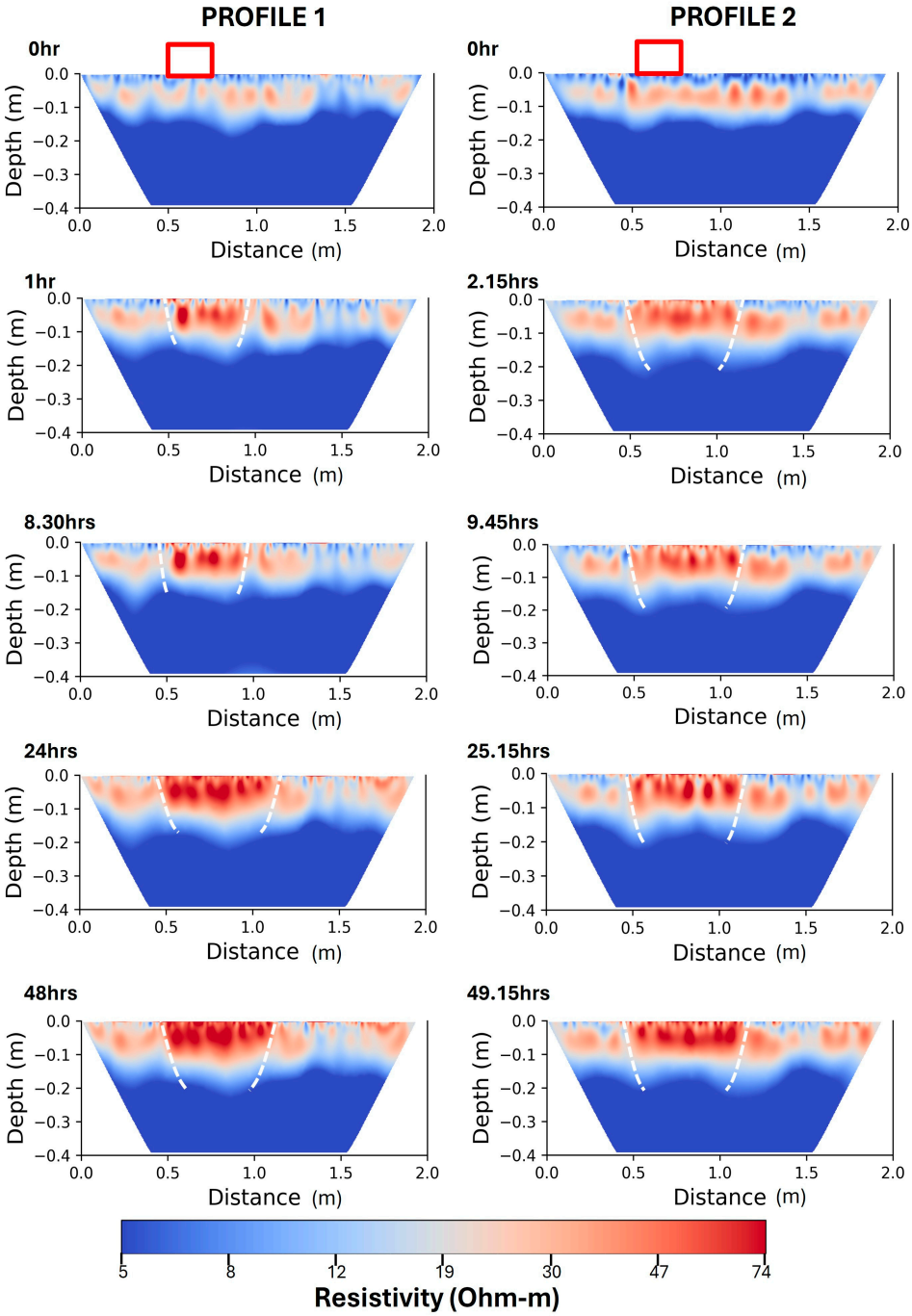

Figure 6. Two-dimensional resistivity inversion results taken across Profiles 1 and 2 for unsaturated salt-impacted sand with a salt concentration of 85 mS/cm during the crude oil spill experiment. Five separate measurements were taken at different times for over 49.15 h using a dipole–dipole array. The red box at the top of the profile shows the crude oil spill surface location between x = 60 cm and x = 75 cm. The white-dashed lines show the left and right boundaries of the crude oil contaminant front.

3.2. Time-Lapse ERI Inversion Results

The effect of crude oil spillage on resistivity across four porewater electrical conductivities (0.6 mS/cm, 20 mS/cm, 50 mS/cm, and 85 mS/cm) was investigated using a time-lapse resistivity inversion. Figures 7–10 show the timelapse inversion results for the four different porewater electrical conductivities. For the baseline resistivity at a depth of 0.2 m, a significant reduction in resistivity was observed as the porewater electrical conductivity level increased. With a 3330% increase in fluid conductivity, a 1750% reduction in resistivity was

observed. A further 190% reduction in resistivity was observed when fluid conductivity increased from 0.6 mS/cm to 20 mS/cm. A 233% reduction in resistivity was observed when the fluid conductivity increased from 50 mS/cm to 85 mS/cm. At a greater depth of 0.35 m, the reductions in resistivity followed a similar trend but with some variations in magnitude compared to the 0.2 m depth. A reduction of 1069% was observed when fluid conductivity increased from 0.6 mS/cm to 20 mS/cm. This was further reduced to 385% when the fluid conductivity increases from 50 mS/cm to 85 mS/cm. The reduction in resistivity from 50 mS/cm to 85 mS/cm remained at 385%. The results show different trends in resistivity changes over time and at various depths.

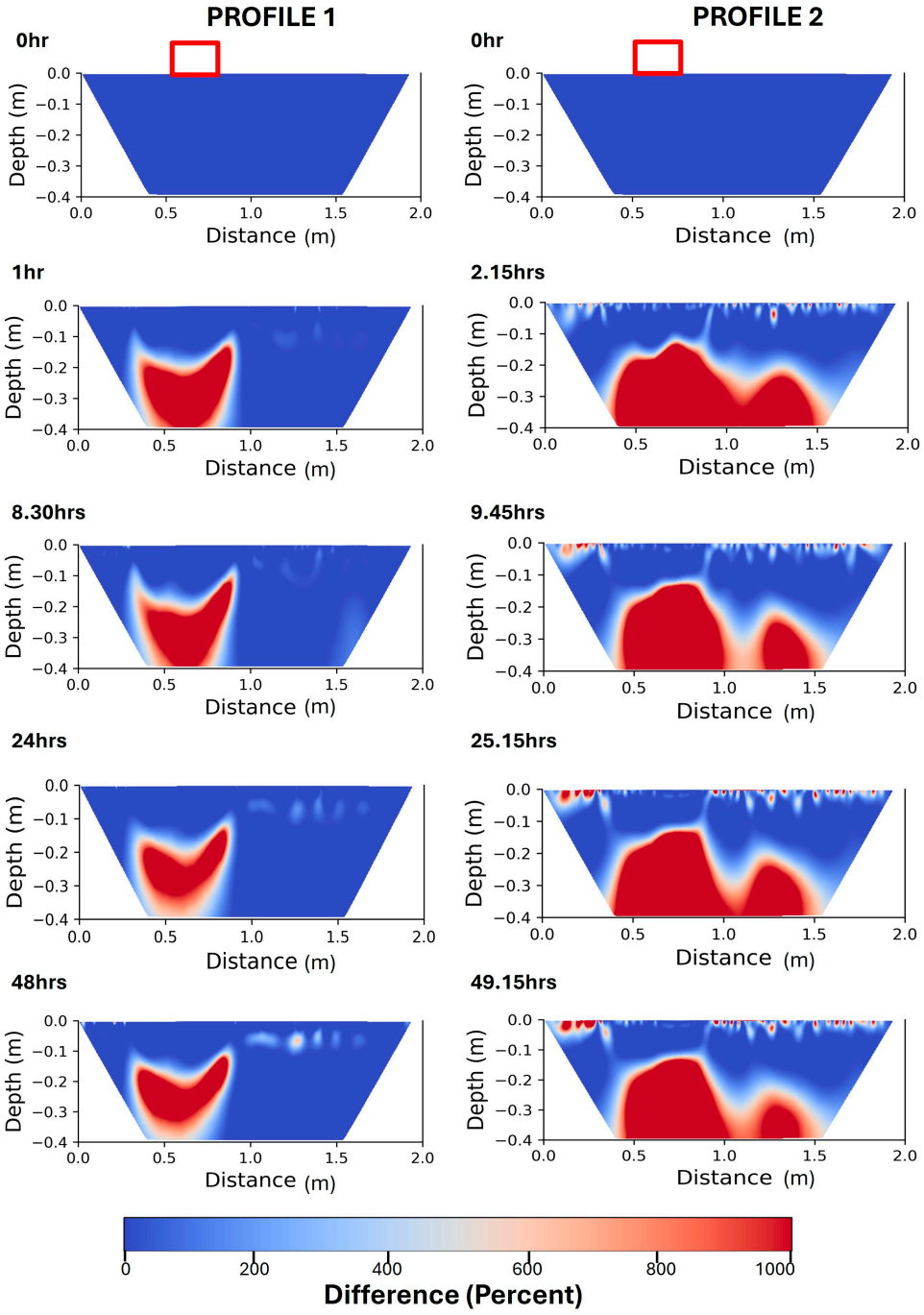

Figure 7. Two-dimensional time-lapse inversion results showing the percentage difference in an unsaturated sand with 0.6 mS/cm concentration, from 0 h to 49.15 h using a dipole–dipole array. The red box at the top of the profile shows the crude oil spill surface location between x = 60 cm and x = 75 cm.

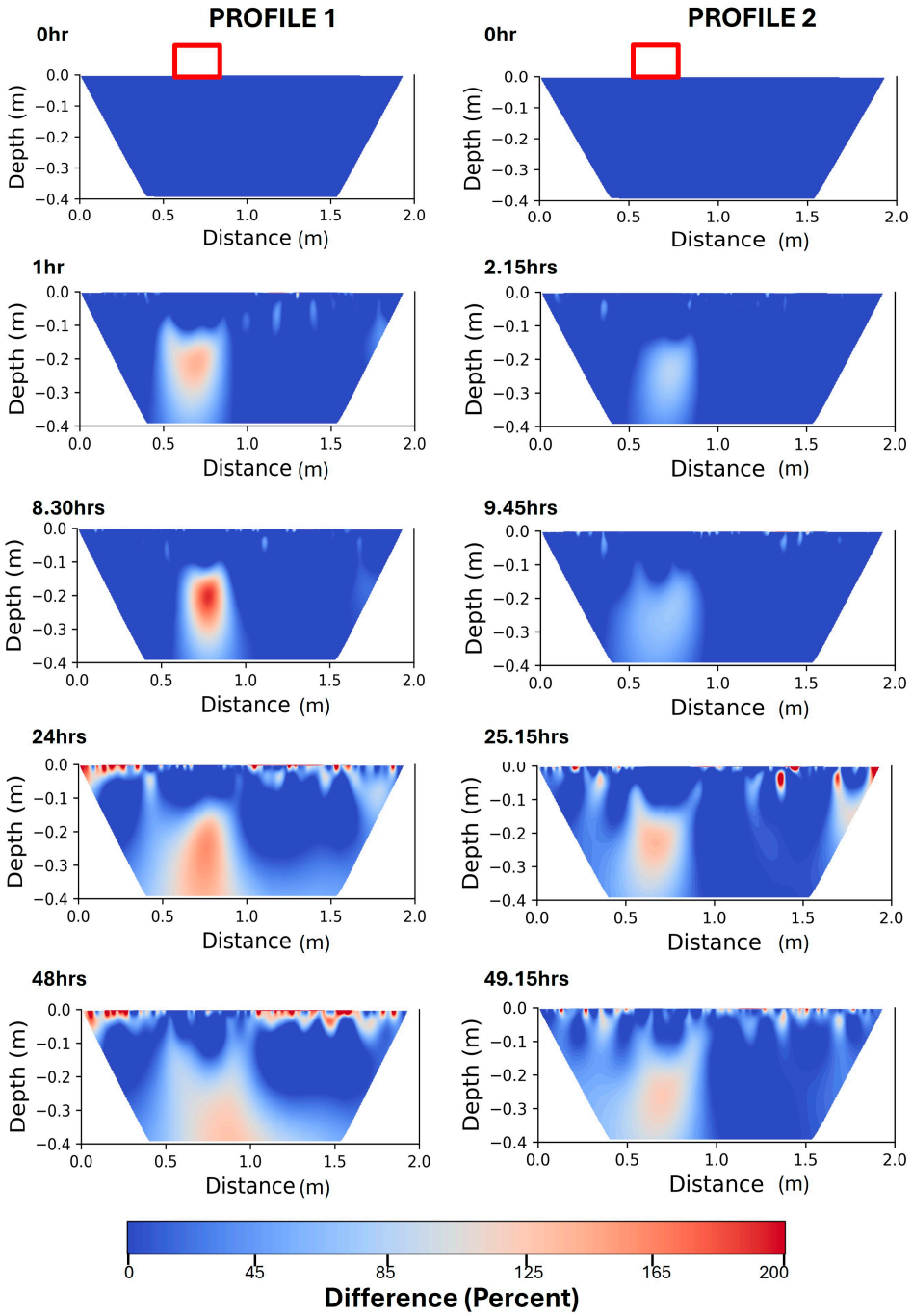

Figure 8. Two-dimensional time-lapse inversion results showing the percentage difference in an unsaturated salt-impacted sand with salt concentration of 20 mS/cm from 0 h to 49.15 h using a dipole–dipole array. The red box at the top of the profile shows the crude oil spill surface location between x = 60 cm and x = 75 cm.

For a low porewater conductivity (0.6 mS/cm), Figure 7 shows an increase in resistivity (reddish zone) at depths between 0.2 and 0.4 m towards the right beneath the spill zone. One hour after spillage, the resistivity rose by 850% directly beneath the spill zone, and after 8 h, the percentage difference increased to 920%. The percentage difference in resistivity reached a peak of 960% after 48 h. For the 20 mS/cm concentration, an initial increase in resistivity was also observed, but at a lower magnitude than the 0.6 mS/cm concentration. At 0.1 m depth, one hour post-spillage showed an initial rise of 200%, then a minor drop of 2% after 8 h. By the end of the experiment which lasted for 48 h, the resistivity increased

to an average of 280%. At a 0.2–0.4 m depth, the resistivity increased by 150% within one hour. After 8 h, a notable drop in resistivity to 67% was observed and remained relatively constant up to 48 h.

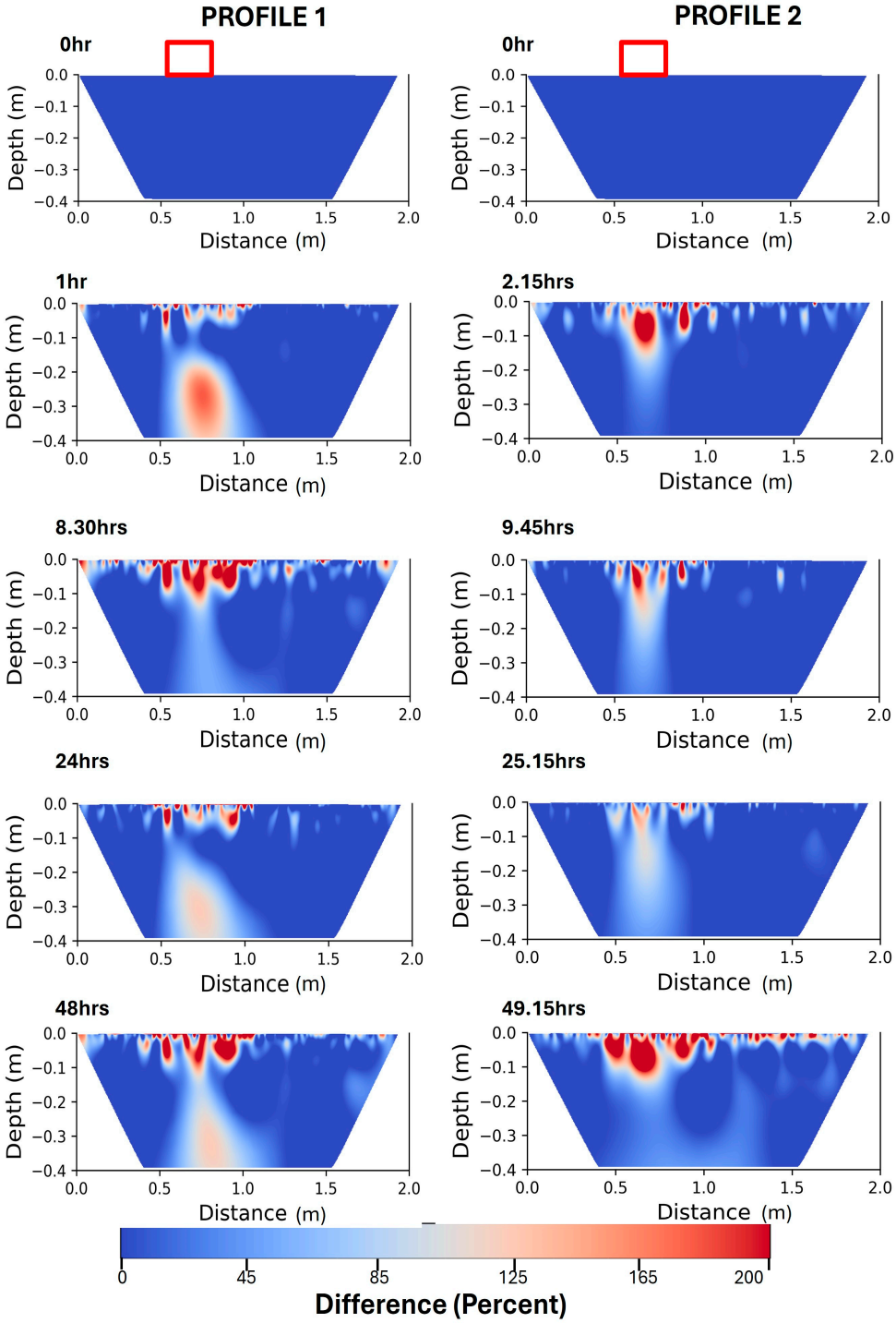

Figure 9. Two-dimensional time-lapse inversion result showing the percentage difference in an unsaturated salt-impacted sand with salt concentration of 50 mS/cm from 0 h to 49.15 h using a dipole–dipole array. The red box at the top of the profile shows the crude oil spill surface location between x = 60 cm and x = 75 cm.

However, unlike 0.6 mS/cm and 20 mS/cm concentrations, the maximum change in resistivity occurred at a depth of 0.1 m. For 50 mS/cm concentration at 0.1 m depth, an

initial 20% rise in resistivity one-hour post-spillage was recorded. After eight hours, the resistivity increased to an average of 182% after 8 h. However, at 0.2–0.4 m depth, resistivity increased 130% within one hour, but dropped to 73% after 8 h, and remained relatively constant for up to 48 h. Similarly, at a shallow depth (0.1 m), for 85 mS/cm concentration, an initial 13% rise was noted after one-hour post-spillage, at 0.1 m depth. The resistivity increased progressively during the next 48 h, producing a 70% variation. However, at depths 0.2–0.4 m, no appreciable resistivity changes were observed.

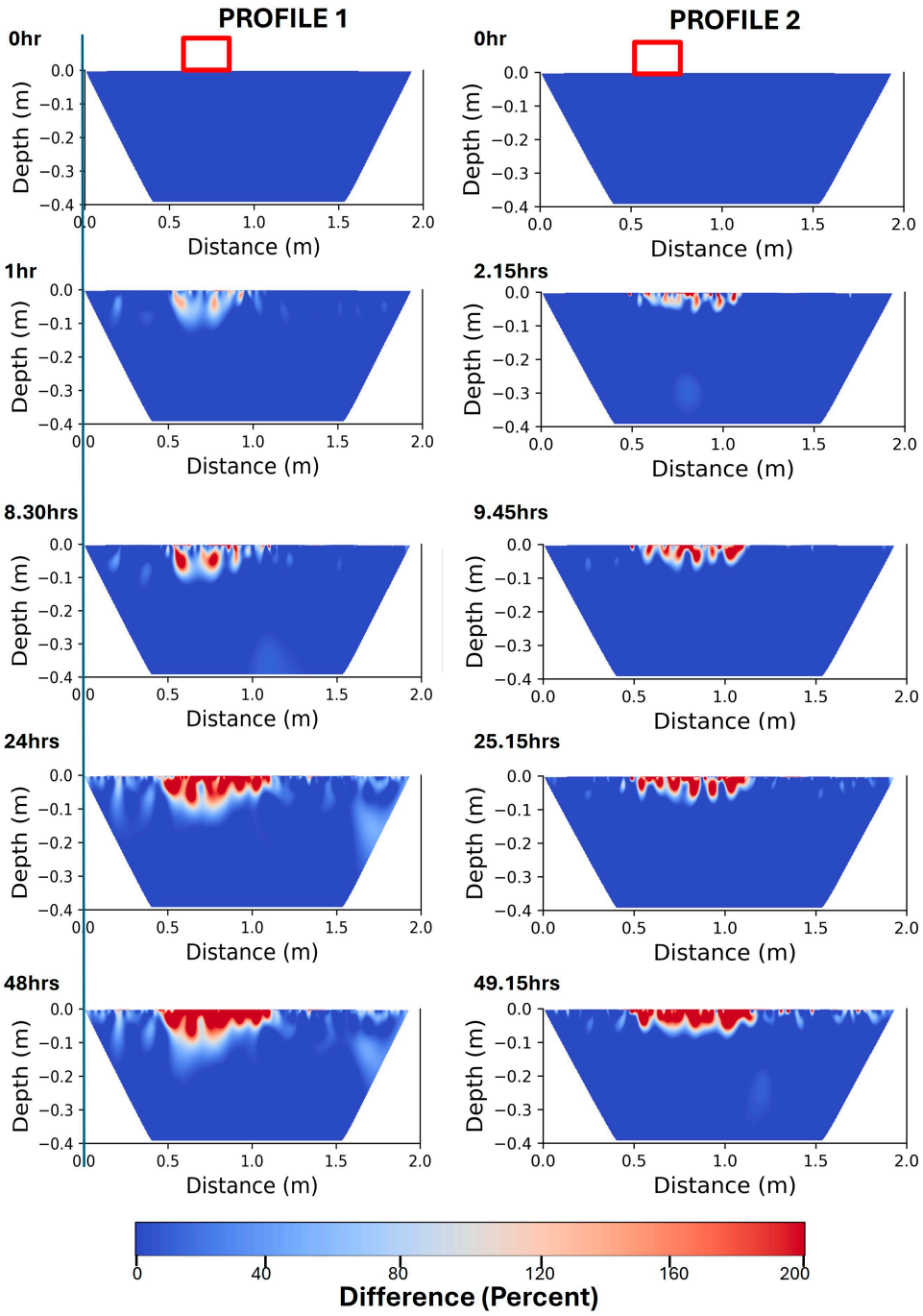

Figure 10. Two-dimensional time-lapse inversion results showing the percentage difference in an unsaturated salt-impacted sand with salt concentration of 85 mS/cm from 0 h to 49.15 h using a dipole–dipole array. The red box at the top of the profile shows the crude oil spill surface location between x = 60 cm and x = 75 cm.

4. Discussion

4.1. Electrical Resistivity Imaging of Crude Oil Distribution

This study highlights the capability of ERI to image the distribution of crude oil contamination in unsaturated coastal sandy soils under varying salinity. This study provided information on the complex interaction between crude oil, water, and the subsurface structure that controls the crude oil migration in unsaturated coastal sands. Background ERI measurements over the homogeneous sand in the sandbox prior to the simulated crude oil spillage show a two-layer resistivity stratification for all four fluid conductivities (Figure 2). This stratification reflects the variation in moisture contents caused by gravity-induced drainage, where the pore fluid moved vertically downward. This resulted in a two-layer resistivity structure with a high resistivity at the upper section (0–0.2 m) and a low resistivity in the lower section (0.2–0.4 m). The observed stratification is consistent with the findings of Costall et al. [41], who observed similar stratification in their ERI studies associated with changes in pore fluid salinity. This mimics natural variations that may arise in coastal beach sands, with strong effects from gravity-induced moisture distribution. While the sand's physical characteristics may be uniform, resistivity models can capture small-scale variation in moisture and salinity contents with depth. A related practical scenario is the distribution of soil moisture and salinity contents after a saltwater overwash along coastal areas. Also, a nonlinear relationship between pore fluid conductivity and resistivity was observed. As fluid conductivity increased from 0.6 mS/cm to 20 mS/cm (a 3330% increase), the resulting resistivity values correspond to a resistivity reduction of approximately 1500%. However, as fluid conductivity increased from 50 mS/cm to 85 mS/cm (70% increase), the rate of resistivity reduction became less pronounced (14%). This finding aligns with the work of Lu et al. [42], who also reported that electrical resistivity decreases nonlinearly with an increase in porewater salinities.

While ERI remains a powerful tool for imaging subsurface crude oil contamination and fluid dynamics, its application in environments with varying salinity, such as coastal interfaces [14], needs a careful consideration of the nonlinear salinity–resistivity relationship [43]. This nonlinear relationship introduces ambiguity in the interpretation of electrical resistivity data, as ERI did not represent the expected resistivity decrease that corresponds to an increase in salinity at higher concentrations. In unsaturated coastal sands, crude oil migration is controlled by the permeability of the sand [2], gravity, viscosity, capillary forces, and the density of crude oil [44,45]. Since crude oil is a non-conductive fluid, an increase in resistivity is expected when it displaces the more conductive pore fluids. However, the magnitude of this increase in resistivity varies depending on the in situ fluid conductivities and the volume of crude oil present in the pores. Our ERI result captures the resistivity increase as crude oil migrates through the sand unit. The increase in resistivity was more pronounced for lower salinity measurement, while at higher salinity, the resistivity variation was more subtle. For all four fluid conductivities, resistivity anomalies became more defined over time as crude oil displaced more of the pore fluid. This is consistent with the results by Atekwana et al. [46], who demonstrated that resistivity variations in contaminated environments are highly dependent on the conductivity of pore fluids. However, the resistivity contrast was lower in higher salinity conditions, suggesting that oil migration may be less effective in displacing saline water, potentially due to changes in oil viscosity and/or interactions with salinity.

Although the migration of crude oil may be impeded at high salinity conditions due to reduced permeability, this does not eliminate the possibility that some crude oil still migrates to deeper depths (0.2–0.4 m). However, the ERI method fails to detect the resistivity contrast, as little to no changes in resistivity were observed (Figure 11; D1–D4). This further confirms the study of Werkema et al. [47], who reported that high salinity in the subsurface diminished the efficacy of geophysical methods like ERI for detecting hydrocarbon contamination. These findings emphasize the need to account for salinity when using ERI for monitoring subsurface crude oil distribution, particularly in coastal regions where saltwater intrusion is common. The results demonstrate that increased salt concentration reduces the contrast between crude oil and pore fluid resistivity. This

reduction, in contrast, significantly impacts the ability to delineate crude oil plumes using ERI, especially in high-salinity environments. This study thus established that high salinity produces a smaller resistivity contrast, which seems counterintuitive given that oil has higher resistivity. This reduction in resistivity contrast arises due to the dominance of conductive zones formed by saline water, which mask the resistive response expected from the presence of crude oil. The presence of salt significantly increases the ionic concentration in pore fluids, enhancing the overall conductivity of the medium. As a result, even when crude oil occupies a portion of the pore space, it does not contribute to an electrical current flow. The current instead flows preferentially through the highly conductive saline fluid. These findings challenge traditional assumptions that high contrast in the electrical properties of two materials produces more interpretable geophysical anomalies. This result thus contradicts those assumptions, as the sensitivity of electrical resistivity imaging to oil contamination is significantly reduced in high-salinity environments, thus highlighting the limitation of conventional resistivity methods in subsurface imaging in such environments.

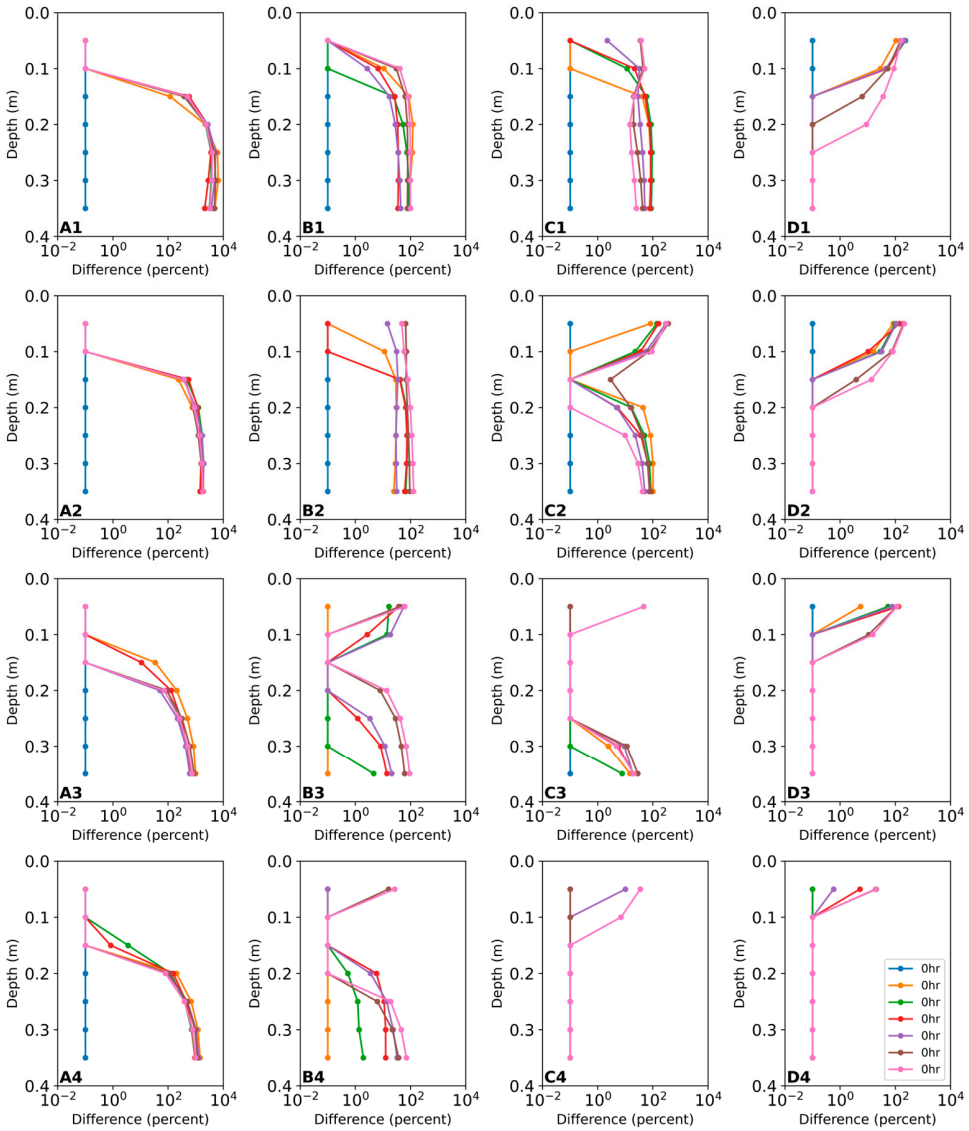

Figure 11. Scattered plots showing variations in percentage difference in resistivity with depth for an unsaturated sand extracted from inverted resistivity model for (**A1**–**A4**) 0.6 mS/cm, at x = 0.5 m, 0.9 m, 1.1 m, and 1.3 m, respectively; (**B1**–**B4**) 20 mS/cm, at x = 0.5 m, 0.9 m, 1.1 m, and 1.3 m, respectively; (**C1**–**C4**) 50 mS/cm at x = 0.5 m, 0.9 m, 1.1 m, and 1.3 m, respectively; and (**D1**–**D4**) 85 mS/cm at x = 0.5 m, 0.9 m, 1.1 m, and 1.3 m, respectively.

Furthermore, the observed decrease in resistivity over time in areas away from the spill zone is consistent with the increase in saturation as crude oil infiltration pushes pore fluid outward (Figure 3). This behavior is comparable to the observations of [48], who reported the formation of low resistivity zones adjacent to contaminant plumes due to increased water saturation. The development of these localized zones of increased saturation reflects the dynamic environment created by crude oil migration, even in seemingly homogenous systems. ERI offers several advantages over traditional contaminant imaging techniques, such as borehole sampling or other point measurements [49]. ERI's ability to provide continuous, high-resolution spatial data allows for a more comprehensive understanding of contaminant migration patterns [50]. Unlike point measurements, which can miss key details of subsurface structures, ERI captures the heterogeneity of the environment, offering a more complete picture of contaminant behavior. However, there is a need for ERI to be used in conjunction with other methods, such as induced polarization (IP), to improve the monitoring of crude oil contaminants in saline subsurface conditions [51]. IP is sensitive to the electrochemical processes occurring at the electrical double layer (EDL), which forms the interface between mineral grains and pore fluids. Unlike resistivity, which is dominated by the conductive pathways of pore fluid, IP can capture the subtle changes in the electrochemical behavior at the EDL, providing a more sensitive response to the presence of oil contaminants. By integrating ERI with complementary techniques, a more robust assessment of contaminant migration can be achieved, leading to better-informed decision making for remediation efforts.

4.2. Influence of Salt Concentration Variations on Crude Oil Migration

The findings of this study highlight the influence of varying fluid conductivity on crude oil contaminant migration in coastal environments. At lower fluid conductivities (0.6 mS/cm), the resistivity contrast between crude oil and pore water was more pronounced (Figures 7 and 8)), making it easier to detect and map oil migration pathways. However, at higher salt concentrations (85 mS/cm) (Figures 9 and 10), the crude oil plume exhibited less distinct boundaries, making it challenging to differentiate between contaminated and uncontaminated zones. Similarly to studies conducted by Sauck [52], our experiments revealed that the migration patterns of crude oil vary vertically and laterally, depending on the salinity of the pore water. Vertically, resistivity contrasts at depth were more detectable at lower salinity conditions (e.g., 0.6 mS/cm, 20 mS/cm, and 50 mS/cm) as crude oil migrated more profoundly into the sand column (Figure 11; A1–A4, B1–B4, C1–C3). However, at higher salinity levels (e.g., 85 mS/cm), crude oil migration was confined to shallower depths, with resistivity anomalies appearing within the top 0.2 m of the sand column (Figure 11; D1–D4). This is in line with previous studies that have shown that high salinity can hinder the downward migration of hydrocarbons, resulting in more surface-level contamination [52]. The significant increase in resistivity at depth for low concentration shows a dominant vertical migration due to gravity and reduced oil–water interfacial tension. Lateral migration observations also corroborate findings from a study by Sun et al. [53], who demonstrated that crude oil tends to spread more extensively at depth in lower salinity environments, producing broader resistivity anomalies. In contrast, in high-salinity environments, the lateral spread of crude oil was mainly confined to the top of the sandbox (Figure 11; D1–D4), likely due to the decreased mobility of crude oil in the presence of saline pore water. The presence of a high concentration of salt in the pore fluid enhances the trapping of crude oil, thereby impeding its downward migration; this could also be a result of changes in capillary forces and the reduction in the density variation between the pore fluids [54]. This leads to a high retention time at shallow depths, eventually increasing the lateral migration of crude oil.

The presence of salt can alter the pore structure and fluid distribution within the subsurface, thereby impacting permeability. In low-salinity conditions, the crude oil migrated more freely, indicating higher permeability and less resistance to flow. In contrast, higher salt concentrations appeared to restrict crude oil movement, likely due to changes in

pore water properties such as increased density and viscosity. These changes can result in reduced permeability, limiting the extent of crude oil migration and leading to more localized oil distributions. Deng et al. [55] reported a similar observation where they observed significant resistivity contrast in low-permeability lenses compared to high-permeable lenses. This suggests that crude oil may be more likely to accumulate in specific regions in environments with higher salinity, potentially making it more difficult to remediate. These findings highlight the importance of permeability characterization when assessing crude oil migration in coastal environments, as the presence of salt can significantly alter permeability. Revil et al. [56] emphasized the role of permeability in controlling contaminant distribution in porous media. Our findings demonstrate that, even in relatively homogenous sand media, slight variations in packing density can significantly impact permeability. This highlights the importance of characterizing permeability in contaminant studies, as micro-scale heterogeneities can significantly influence the distribution and behavior of contaminants.

The temporal monitoring of resistivity changes further revealed the dynamic nature of crude oil migration in different salinity environments. In high-salinity environments, minimal changes in resistivity were observed over the 48 h monitoring period, suggesting that the oil had become immobilized shortly after the spill. This is in contrast with lower salinity environments, where ongoing resistivity decreases indicate continued oil migration. This temporal variability is crucial for understanding the long-term behavior of contaminant plumes, as it highlights the importance of time-lapse ERI studies in capturing the full extent of oil migration. Previous studies, such as those by [57], have similarly emphasized long-term monitoring to accurately assess contaminant dynamics, particularly in complex environments like coastal sands.

Understanding how crude oil migration is influenced by salinity has direct implications for remediation strategies. In Nigeria, remediation solutions have frequently utilized the enhanced natural attenuation (RENA) method. Nevertheless, the extent and complexity of contamination in the Niger Delta have demonstrated that the applicability of RENA is insufficient [58]. Although the transition to more economical and ecologically friendly options like phytoremediation and active bioremediation seems promising, the problem of varying salinity levels in coastal areas should be addressed [59]. The fluctuation in salinity poses considerable challenges, especially in biological processes such as microbial bioremediation and phytoremediation. Variations in salinity disturb microbial communities and plant-mediated degradation processes, impacting the stability and functionality of oil-degrading microorganisms [60]. For example, the activity of microorganisms that are adapted to either freshwater or saline conditions is inhibited by increased salinity levels [61–63]. This variability can result in significant amounts of crude oil remaining untreated, extending contamination in vulnerable ecosystems and causing uneven or inadequate remediation efforts.

As previously mentioned, the reduction in the capacity of ERI in imaging crude oil contaminants in a high-salinity setting presents an additional obstacle. This may lead to inaccuracies in defining the contamination plumes in regions. Given these constraints, there is a need to create adaptable, site-specific, multidisciplinary strategies for crude oil contaminant clean-ups. The influence of salt concentration on oil migration must be considered when designing remediation strategies. In areas with high salt concentrations, the restricted migration of crude oil suggests that remediation efforts may need to focus on more localized treatments, targeting areas where oil is trapped due to reduced permeability and capillary forces. On the other hand, in areas with lower salt concentrations, crude oil migration is more extensive, meaning that remediation strategies must address a larger area. The more dispersed contamination in these environments may require more widespread remediation efforts. Also, incorporating the halophilic microbial consortia, selecting salt-tolerant plant species for phytoremediation, and applying integrated geophysical techniques will go a long way towards increasing the success rate of the remediation exercise.

Although these results provide an insightful analysis of ERI applications for subsurface imaging, this study has limitations. First, the study did not characterize the effect of temperature on resistivity measurements since temperature-induced changes might introduce noise into ERI data and impact the correct identification of crude oil contamination. Also, the variation in soil moisture content at different depths was not addressed, potentially reducing the accuracy of resistivity variations. This limitation emphasizes the need for in situ soil moisture assessments at various depths to improve ERI measurement calibration. Furthermore, incorporating IP measurements improves the characterization of crude oil contamination. Crude oil contamination modifies the charge distribution at the mineral–fluid interface (electrical double layer), and this approach can accurately measure the consequent electrical response [64,65]. This technique would facilitate the identification of regions with chargeability signatures, providing differentiation between places contaminated by crude oil and those impacted by saline water. The incorporation of IP could enhance the precision of contaminant imaging [51]. Combining cutting-edge geophysical methods like IP with in-situ moisture monitoring will help to better capture the pollutant distribution and increase the success of remedial actions in these challenging environments. Future studies will investigate these limitations alongside the interaction between salt concentration, permeability, and pollutant behavior to further improve remedial plans for coastal environments.

5. Conclusions

This study demonstrates the capability of ERI as a non-invasive geophysical technique for characterizing the distribution of crude oil contaminants in coastal sands under varying salinity conditions. The time-lapse ERI used in this study is a good approach to studying the electrical response of crude oil distribution in sandy soils under varying salt concentrations. This study shows that a nonlinear relationship exists between pore fluid conductivity and the measured bulk electrical resistivity of the crude-oil-contaminated sand as electrical resistivity decreases nonlinearly with increased porewater salinities. Our study reveals that increased salinity reduced the sensitivity of electrical resistivity measurements in detecting crude oil contamination. Also, vertical resistivity contrasts were more detectable at lower salinity conditions. Meanwhile, in high-salinity conditions, the lateral spread of crude oil is dominant as crude oil contaminants are mainly confined to shallow depths. This restriction in crude oil migration is likely due to changes in pore water properties, such as increased density and viscosity, as well as reduced permeability. Thus, there is a need to account for salinity when using ERI for crude oil contaminant monitoring, particularly in coastal regions where saltwater intrusion is common.

By integrating ERI data with other site-specific information, such as permeability measurements and hydrological data, researchers can better understand the factors controlling crude oil migration in coastal sands. This integration is essential for developing accurate contaminant transport models and designing effective remediation strategies. In conclusion, ERI provides a reliable tool for imaging crude oil migration in unsaturated coastal sands, offering detailed insights into the subsurface dynamics of oil plumes and informing more effective environmental management practices. Future research should continue exploring the relationship between salt concentration, permeability, and contaminant behavior to further refine remediation approaches in coastal settings. A continued investigation into how varying salinity levels influence the long-term dynamics of crude oil plumes will be crucial for developing effective remediation strategies tailored to the unique challenges of coastal environments. Additionally, integrating other geophysical methods alongside ERI may help overcome some of the limitations of high salinity, providing a more comprehensive understanding of contaminant distribution and movement.

Author Contributions: Conceptualization, M.A.A., M.A.O. and K.O.D.; methodology M.A.A., M.A.O. and K.O.D.; software, M.A.A., M.A.O. and K.O.D.; formal analysis, M.A.A. and K.O.D.; investigation, M.A.A., M.A.O. and K.O.D.; resources, M.A.O. and K.O.D.; writing—original draft preparation, M.A.A.; writing—review and editing, M.A.O. and K.O.D.; visualization, M.A.A., M.A.O. and K.O.D.; supervision, M.A.O. and K.O.D.; project administration, M.A.A., M.A.O. and K.O.D.; funding acquisition, M.A.A., M.A.O. and K.O.D. All authors have read and agreed to the published version of the manuscript.

Funding: This research was funded by the African Union through the Pan African University Initiative, the Society of Exploration Geophysicists (SEG): 2023 and 2024 SEG Foundation/Chevron Scholarship, and the American Association of Petroleum Geologists (AAPG): 2022 and 2023 AAPG Grant-in-aid. This study also benefited from a research collaboration between the Hydro & Environmental Geophysics Research Group at the University of Toledo, Ohio, USA, and the Hydrogeophysics Research Team at the University of Ibadan, Nigeria.

Data Availability Statement: The raw data supporting the conclusions of this article will be made available by the authors upon request.

Conflicts of Interest: The authors declare no conflicts of interest. The funders had no role in the design of the study; in the collection, analyses, or interpretation of data; in the writing of the manuscript; or in the decision to publish the results.

References

1. Dai, C.; Han, Y.; Duan, Y.; Lai, X.; Fu, R.; Liu, S.; Leong, K.H.; Tu, Y.; Zhou, L. Review on the contamination and remediation of polycyclic aromatic hydrocarbons (PAHs) in coastal soil and sediments. *Environ. Res.* **2022**, *205*, 112423. [CrossRef] [PubMed]
2. Jekayinfa, S.M.; Oladunjoye, M.A.; Doro, K.O. A review of the occurrence, distribution, and impact of bitumen seeps on soil and groundwater in parts of southwestern Nigeria. *Environ. Monit. Assess.* **2023**, *195*, 351. [CrossRef] [PubMed]
3. Adeniran, M.A.; Oladunjoye, M.A.; Doro, K.O. Soil and groundwater contamination by crude oil spillage: A review and implications for remediation projects in Nigeria. *Front. Environ. Sci.* **2023**, *11*, 1137496. [CrossRef]
4. Laignel, B.; Vignudelli, S.; Almar, R.; Becker, M.; Bentamy, A.; Benveniste, J.; Birol, F.; Frappart, F.; Idier, D.; Salameh, E.; et al. Observation of the coastal areas, estuaries and deltas from space. *Surv. Geophys.* **2023**, *44*, 1309–1356. [CrossRef]
5. Adebayo, M.B.; Bailey, V.L.; Chen, X.; Hopple, A.M.; Jiang, P.; Li, B.; Li, Z.; Martin-Hayden, J.M.; Megonigal, J.P.; Regier, P.J.; et al. A hydrogeophysical framework to assess infiltration during a simulated ecosystem-scale flooding experiment. *J. Hydrol.* **2023**, *626*, 130243. [CrossRef]
6. Basack, S.; Loganathan, M.K.; Goswami, G.; Khabbaz, H. Saltwater intrusion into coastal aquifers and asso-ciated risk management: Critical review and research directives. *J. Coast. Res.* **2022**, *38*, 654–672. [CrossRef]
7. Essaid, H.I.; Bekins, B.A.; Cozzarelli, I.M. Organic contaminant transport and fate in the subsurface: Evolution of knowledge and understanding. *Water Resour. Res.* **2015**, *51*, 4861–4902. [CrossRef]
8. Zhu, Z.; Merlin, F.; Yang, M.; Lee, K.; Chen, B.; Liu, B.; Cao, Y.; Song, X.; Ye, X.; Li, Q.K.; et al. Recent advances in chemical and biological degradation of spilled oil: A review of dispersants application in the marine envi-ronment. *J. Hazard. Mater.* **2022**, *436*, 129260. [CrossRef]
9. McGenity, T.J.; Folwell, B.D.; McKew, B.A.; Sanni, G.O. Marine crude-oil biodegradation: A central role for in-terspecies interactions. *Aquat. Biosyst.* **2012**, *8*, 10. [CrossRef]
10. Kong, K.; Shao, S. Effect of wettability on the variation of resistivity characteristics during diesel oil infiltration into the unsaturated zone. *Environ. Earth Sci.* **2023**, *82*, 552. [CrossRef]
11. Iwai, C.B.; Oo, A.N.; Topark-ngarm, B. Soil property and microbial activity in natural salt affected soils in an alternating wet–dry tropical climate. *Geoderma* **2012**, *189*, 144–152. [CrossRef]
12. Hajabbasi, M.A. Importance of soil physical characteristics for petroleum hydrocarbons phytoremediation: A re-view. *Afr. J. Environ. Sci. Technol.* **2016**, *10*, 394–405.
13. Kakati, A.; Sangwai, J.S. Wettability alteration of mineral surface during low-salinity water flooding: Role of salt type, pure alkanes, and model oils containing polar components. *Energy Fuels* **2018**, *32*, 3127–3137. [CrossRef]
14. Hopple, A.M.; Doro, K.O.; Bailey, V.L.; Bond-Lamberty, B.; McDowell, N.; Morris, K.A.; Myers-Pigg, A.; Pennington, S.C.; Regier, P.; Rich, R.; et al. Attaining freshwater and estuarine-water soil saturation in an ecosystem-scale coastal flooding experiment. *Environ. Monit. Assess.* **2023**, *195*, 425. [CrossRef] [PubMed]
15. Werner, A.D.; Bakker, M.; Post, V.E.; Vandenbohede, A.; Lu, C.; Ataie-Ashtiani, B.; Simmons, C.T.; Barry, D.A. Seawater intrusion processes, investigation and management: Recent advances and future challenges. *Adv. Water Resour.* **2013**, *51*, 3–26. [CrossRef]
16. Riser-Roberts, E. *Remediation of Petroleum Contaminated Soils: Biological, Physical, and Chemical Processes*; CRC Press: Boca Raton, FL, USA, 2020.
17. Nyári, Z.; Kanlı, A.I.; Stickel, J.; Tillmann, A. The use of non-conventional CPTe data in determination of 3-D electrical resistivity distribution. *J. Appl. Geophys.* **2010**, *70*, 255–265. [CrossRef]

18. Jekayinfa, S.M.; Oladunjoye, M.A.; Doro, K.O. Effects of groundwater flow on the distribution of bitumen contaminants in a shallow coastal plain sand aquifer of the Nigerian Dahomey basin. *J. Afr. Earth Sci.* **2023**, *203*, 104946. [CrossRef]
19. Ossai, I.C.; Ahmed, A.; Hassan, A.; Hamid, F.S. Remediation of soil and water contaminated with petroleum hydrocarbon: A review. *Environ. Technol. Innov.* **2020**, *17*, 100526. [CrossRef]
20. Nadporozhskaya, M.; Kovsh, N.; Paolesse, R.; Lvova, L. Recent advances in chemical sensors for soil analysis: A review. *Chemosensors* **2022**, *10*, 35. [CrossRef]
21. Binley, A.; Cassiani, G.; Deiana, R. Hydrogeophysics: Opportunities and challenges. *Boll. Geofis. Teor. Appl.* **2010**, *51*, 267–284.
22. Gruiz, K. Integrated and efficient characterization of contaminated sites. *Eng. Tools Environ. Risk Manag.* **2016**, *3*, 1–89.
23. Doro, K.O.; Leven, C.; Cirpka, O.A. Delineating subsurface heterogeneity at a loop of River Steinlach using geophysical and hydrogeological methods. *Environ. Earth Sci.* **2013**, *69*, 335–348. [CrossRef]
24. Driba, D.L.; Emmanuel, E.D.; Doro, K.O. Predicting wetland soil properties using machine learning, geophysics, and soil measurement data. *J. Soils Sediments* **2024**, *24*, 2398–2415. [CrossRef]
25. Vogelsang, D. *Environmental Geophysics: A Practical Guide*; Springer Science & Business Media: New York, NY, USA, 2012.
26. Cassiani, G.; Boaga, J.; Barone, I.; Perri, M.T.; Deidda, G.P.; Vignoli, G.; Strobbia, C.; Busato, L.; Deiana, R.; Rossi, M.; et al. Ground-based remote sensing of the shallow subsurface: Geophysical methods for environmental applications. In *Developments in Earth Surface Processes*; Elsevier: Amsterdam, The Netherlands, 2020; Volume 23, pp. 55–89.
27. Atekwana, E.A.; Atekwana, E.A. Geophysical signatures of microbial activity at hydrocarbon contaminated sites: A review. *Surv. Geophys.* **2010**, *31*, 247–283. [CrossRef]
28. Emmanuel, E.D.; Lenhart, C.F.; Weintraub, M.N.; Doro, K.O. Estimating soil properties distribution at a restored wetland using electromagnetic imaging and limited soil core samples. *Wetlands* **2023**, *43*, 39. [CrossRef]
29. Binley, A.; Hubbard, S.S.; Huisman, J.A.; Revil, A.; Robinson, D.A.; Singha, K.; Slater, L.D. The emergence of hydrogeophysics for improved understanding of subsurface processes over multiple scales. *Water Resour. Res.* **2015**, *51*, 3837–3866. [CrossRef] [PubMed]
30. Adeniran, M.A.; Oladunjoye, M.A.; Doro, K.O. Electrical resistivity imaging of crude oil contaminant in coastal soils–A laboratory sandbox study. *J. Appl. Geophys.* **2024**, *230*, 105516. [CrossRef]
31. Aladejana, J.A.; Kalin, R.M.; Sentenac, P.; Hassan, I. Groundwater quality index as a hydrochemical tool for monitoring saltwater intrusion into coastal freshwater aquifer of Eastern Dahomey Basin, Southwestern Nigeria. *Groundw. Sustain. Dev.* **2021**, *13*, 100568. [CrossRef]
32. Ukenye EA and Taiwo IA, Studies on the physico chemical status and biological characteristics of some rivers in Nigerian coastal states. *Int. J. Fish. Aquat. Stud.* **2019**, *7*, 192–196.
33. Aladejana, J.A.; Kalin, R.M.; Sentenac, P.; Hassan, I. Hydrostratigraphic Characterisation of Shallow Coastal Aquifers of Eastern Dahomey Basin, S/W Nigeria, Using Integrated Hydrogeophysical Approach; Implication for Saltwater Intrusion. *Geosciences* **2020**, *10*, 65. [CrossRef]
34. Yusuf, M.A.; Abiye, T.A.; Ibrahim, K.O.; Ojulari, B.A. Assessment of saltwater–freshwater interactions using water samples and borehole logging information in the Lagos coastal region, Nigeria. *Environ. Earth Sci.* **2021**, *80*, 1–19. [CrossRef]
35. Ohwoghere-Asuma, O.; Aweto, K.E.; Ovwamuedo, G.; Ugbome, D. Surficial Survey of Unstressed Aquifers for Saltwater-freshwater Interaction using 2D Inverse Resistivity Model and Saltwater Markers in the Coastal Area of Ogheye in the Niger Delta Basin, Nigeria. *Jordan J. Earth Environ. Sci.* **2023**, *14*, 195–202.
36. Abam, T.K.S.; Nwankwoala, H.O. Hydrogeology of Eastern Niger Delta: A Review. *J. Water Resour. Prot.* **2020**, *12*, 741–777. [CrossRef]
37. Reynolds, J.M. *An Introduction to Applied and Environmental Geophysics*; John Wiley & Sons: Hoboken, NJ, USA, 2011.
38. Blanchy, G.; Saneiyan, S.; Boyd, J.; McLachlan, P.; Binley, A. ResIPy, an intuitive open source software for complex geoelectrical inversion/modeling. *Comput. Geosci.* **2020**, *137*, 104423. [CrossRef]
39. Doro, K.O.; Emmanuel, E.D.; Adebayo, M.B.; Bank, C.G.; Wescott, D.J.; Mickleburgh, H.L. Time-lapse electrical resistivity tomography imaging of buried human remains in simulated mass and individual graves. *Front. Envi-Ronmental Sci.* **2022**, *10*, 882496. [CrossRef]
40. Binley, A.; Kemna, A. DC resistivity and induced polarization methods. In *Hydrogeophysics*; Springer: Dordrecht, The Netherlands, 2005; pp. 129–156.
41. Costall, A.; Harris, B.; Pigois, J.P. Electrical resistivity imaging and the saline water interface in high-quality coastal aquifers. *Surv. Geophys.* **2018**, *39*, 753–816. [CrossRef]
42. Lu, Y.; Abuel-Naga, H.; Al Rashid, Q.; Hasan, M.F. Effect of pore-water salinity on the electrical resistivity of partially saturated compacted clay liners. *Adv. Mater. Sci. Eng.* **2019**, *2019*, 7974152. [CrossRef]
43. Cong-Thi, D.; Dieu, L.P.; Caterina, D.; De Pauw, X.; Thi, H.D.; Ho, H.H.; Nguyen, F.; Hermans, T. Quantifying salinity in heterogeneous coastal aquifers through ERT and IP: Insights from laboratory and field investigations. *J. Contam. Hydrol.* **2024**, *262*, 104322. [CrossRef]
44. Francisca, F.M.; Montoro, M.A. Influence of particle size distribution and wettability on the displacement of LNAPL in saturated sandy soils. *J. Environ. Eng.* **2015**, *141*, 04014091. [CrossRef]
45. Boufadel, M.; Geng, X.; An, C.; Owens, E.; Chen, Z.; Lee, K.; Taylor, E.; Prince, R.C. A review on the factors affecting the deposition, retention, and biodegradation of oil stranded on beaches and guidelines for designing laboratory experiments. *Curr. Pollut. Rep.* **2019**, *5*, 407–423. [CrossRef]

46. Atekwana, E.; Atekwana, E.A.; Legall, F.D.; Krishnamurthy, R.V.; Sauck, W.A. Relationship between biodegradation and bulk electrical conductivity. In Proceedings of the 17th EEGS Symposium on the Application of Geophysics to Engineering and Environmental Problems, Colorado Springs, CO, USA, 22–26 February 2004; European Association of Geoscientists & Engineers: Utrecht, The Netherlands, 2004; p. cp-186.
47. Werkema Jr, D.D.; Atekwana, E.A.; Endres, A.L.; Sauck, W.A.; Cassidy, D.P. Investigating the geoelectrical response of hydrocarbon contamination undergoing biodegradation. *Geophys. Res. Lett.* **2003**, *30*. [CrossRef]
48. Koroma, S.; Arato, A.; Godio, A. Analyzing geophysical signature of a hydrocarbon-contaminated soil using geoelectrical surveys. *Environ. Earth Sci.* **2015**, *74*, 2937–2948. [CrossRef]
49. Meng, J.; Dong, Y.; Xia, T.; Ma, X.; Gao, C.; Mao, D. Detailed LNAPL plume mapping using electrical resistivity tomography inside an industrial building. *Acta Geophys.* **2022**, *70*, 1651–1663. [CrossRef]
50. Merioua, A.; Bezzar, A.; Ghomari, F. Non-destructive electrical methods for measuring the physical charac-teristics of porous materials. *J. Nondestruct. Eval.* **2015**, *34*, 13. [CrossRef]
51. Malehmir, A.; Socco, L.V.; Bastani, M.; Krawczyk, C.M.; Pfaffhuber, A.A.; Miller, R.D.; Maurer, H.; Frauenfelder, R.; Suto, K.; Bazin, S.; et al. Near-surface geophysical characterization of areas prone to natural hazards: A review of the current and perspective on the future. *Adv. Geophys.* **2016**, *57*, 51–146.
52. Sauck, W.A. A model for the resistivity structure of LNAPL plumes and their environs in sandy sediments. *J. Appl. Geophys.* **2000**, *44*, 151–165. [CrossRef]
53. Sun, Z.; Mehmani, A.; Torres-Verdín, C. Pore-scale investigation of the electrical resistivity of saturated porous media: Flow patterns and porosity efficiency. *J. Geophys. Res. Solid Earth* **2021**, *126*, e2021JB022608. [CrossRef]
54. Pan, Y.; Zhang, Q.; Yu, Y.; Tong, Y.; Wu, W.; Zhou, Y.; Hou, W.; Yang, J. Three-dimensional migration and resistivity characteristics of crude oil in heterogeneous soil layers. *Environ. Pollut.* **2021**, *268*, 115309. [CrossRef]
55. Deng, Y.; Shi, X.; Xu, H.; Sun, Y.; Wu, J.; Revil, A. Quantitative assessment of electrical resistivity tomography for monitoring DNAPLs migration–Comparison with high-resolution light transmission visualization in laboratory sandbox. *J. Hydrol.* **2017**, *544*, 254–266. [CrossRef]
56. Revil, A.; Kessouri, P.; Torres-Verdín, C. Electrical conductivity, induced polarization, and permeability of the Fontainebleau sandstone. *Geophysics* **2014**, *79*, D301–D318. [CrossRef]
57. Chambers, J.; Ogilvy, R.; Kuras, O.; Cripps, J.; Meldrum, P. 3D electrical imaging of known targets at a controlled environmental test site. *Environ. Geol.* **2002**, *41*, 690–704. [CrossRef]
58. Sam, K.; Coulon, F.; Prpich, G. Management of petroleum hydrocarbon contaminated sites in Nigeria: Current challenges and future direction. *Land Use Policy* **2017**, *64*, 133–144. [CrossRef]
59. Zabbey, N.; Sam, K.; Onyebuchi, A.T. Remediation of contaminated lands in the Niger Delta, Nigeria: Prospects and challenges. *Sci. Total Environ.* **2017**, *586*, 952–965. [CrossRef] [PubMed]
60. Ayyam, V.; Palanivel, S.; Chandrakasan, S.; Ayyam, V.; Palanivel, S.; Chandrakasan, S. Bioremediation: Key to Restore the Productivity of Coastal Areas. In *Coastal Ecosystems of the Tropics-Adaptive Management*; Springer: Berlin/Heidelberg, Germany, 2019; pp. 551–578.
61. Zahran, H.H. Diversity, adaptation and activity of the bacterial flora in saline environments. *Biol. Fertil. Soils* **1997**, *25*, 211–223. [CrossRef]
62. Uko, M.; Udotong, I.; Ofon, U.; Umana, S.; Abraham, N. Effect of hydrocarbon contamination on the microbial diversity of freshwater sediments within akwa ibom state, Nigeria. *J. Chem. Environ. Biol. Eng.* **2020**, *8*, 32. [CrossRef]
63. Zhang, G.; Bai, J.; Zhai, Y.; Jia, J.; Zhao, Q.; Wang, W.; Hu, X. Microbial diversity and functions in saline soils: A review from a biogeochemical perspective. *J. Adv. Res.* **2024**, *59*, 129–140. [CrossRef]
64. Day-Lewis, F.; Singha, K.; Haggerty, R.; Johnson, T.; Binley, A.; Lane, J. *Geoelectrical Measurement of Mul-ti-Scale Mass Transfer Parameters (No. DOE-LANCASTER-SC0001351)*; University of Lancaster: Lancaster, UK, 2014.
65. Kessouri, P.; Johnson, T.; Day-Lewis, F.D.; Wang, C.; Ntarlagiannis, D.; Slater, L.D. Post-remediation geo-physical assessment: Investigating long-term electrical geophysical signatures resulting from bioremediation at a chlorin-ated solvent contaminated site. *J. Environ. Manag.* **2022**, *302*, 113944. [CrossRef]